GPPS | JOURNAL

JOURNAL OF THE GLOBAL POWER AND PROPULSION SOCIETY
journal.gpps.global

Variable turbine geometry for an automotive turbocharger with a small axial turbine

Review article

Article history:
Submission date: 21 November 2024
Acceptance date: 23 July 2025
Publication date: 11 March 2026

***Correspondence:**
CK: kuestner@tfd.uni-hannover.de

Peer review:
Single blind

Keywords:
variable turbine geometry; turbocharger; axial turbine

Citation:
Kuestner C., Helmsen E., and Seume J. R. (2025). Variable turbine geometry for an automotive turbocharger with a small axial turbine. Journal of the Global Power and Propulsion Society. 10: 61–73.
https://doi.org/10.33737/jgpps/208541

Christoph Kuestner[1,*], Eike Helmsen[1], Joerg R. Seume[1]

[1]*Institute of Turbomachinery and Fluid Dynamics, Leibniz Universität Hannover, An der Universität 1, Garbsen, Lower Saxony, Germany*

Abstract

The paper examines the implementation of a variable turbine geometry (VTG) and the reduction of its tip leakage losses in a small axial turbine turbocharger for charging lean-burn internal combustion engines. Due to the small turbine size, a reduction in the number of vanes and a redesign was required to match the design point of the non-adjustable stator. Subsequently, disks were added to the vanes' ends to seal the radial gaps in the VTG. The turbine size prohibited a full sealing on the hub side, leaving small gaps at the leading edge (LE) and trailing edge (TE). To evaluate their influence, three gap configurations of the adjusted design (constant hub gap, partial gaps at LE and TE, and non-gap) were compared with the initial design using CFD simulations. The results showed that the partial gap configuration was able to reduce the maximum mass flow rate deviations at the investigated turbine speed down to 0.8% while maintaining the same turbine efficiencies as the non-gap configuration. Finally, the performance map was evaluated for the partial gap configuration, which showed that the turbine required a slightly larger pivot angle range to meet the specified requirements.

Introduction

The CO_2- and NOx-emissions of internal combustion engines (ICEs) can be significantly reduced by increasing the engine's air-to-fuel ratio λ, which lowers the combustion temperature and increases the engine efficiency (Sens et al., 2018; Zaccardi and Pilla, 2019; Wenz et al., 2021). A downside of this lean-burn technology is the requirement of high turbocharger (T/C) efficiencies and a low rotor inertia of the T/C. Therefore, most lean-burn ICEs feature a two-stage T/C or an electrically-assisted T/C compromising on costs, installation space, and weight like in Clasen et al. (2018) or Luszcz et al. (2018).

These issues were addressed in a previous paper by Sagan et al. (2022a), in which the operating range of the Worldwide harmonized light-vehicles test cycle (WLTC) was covered with air-to-fuel ratios of $\lambda = 2$, whereas the remaining engine operating points were covered with $\lambda = 1$. The results demonstrated that a specially designed single-stage T/C equipped with a small axial turbine was able to significantly improve the lean-burn performance of the ICE, while keeping the rotor inertia low. In its previous state, the turbine was equipped with a wastegate to adapt the boost pressure to the demands of the engine. With the wastegate, the system was able to fulfill the requirements for the entire $\lambda = 1$ operating range and the requirements for $\lambda = 2$ above engine speeds of 2,500 min^{-1}. However, it was found that the turbine's choke

characteristic limits the $\lambda = 2$ operating range for speeds below 2,500 min^{-1} due to an oversized turbine cross-section. Thus, the first objective addressed in this paper is to overcome these limitations by implementing a variable turbine geometry (VTG) with pivoting vanes upstream of the turbine.

State-of-the-art solutions for pivoting vanes in turbomachines typically have a gap at the hub side or at the shroud side of the vanes end, leading to secondary flow losses and a reduction of the machine performance (Benstein and Wood, 1964; Penny, 1964; Berenyi and Raffa, 1979). Understanding and reducing these losses in nozzles (and rotors) is the subject of former research, e.g. in Kammeyer et al. (2010b) or Natkaniec et al. (2011). The relative gap height,

$$\xi_{\text{rel}} = \frac{\xi}{h_{\text{V}}}, \tag{1}$$

was found to be a key factor (Storer and Cumpsty, 1991; Lei et al., 2022). Since the minimal absolut gap height is constrained by the bearings and the thermo-mechanical expansion of the components, small machines show higher relative gap height and, consequently, higher relative losses. Although much effort has been put into reducing and avoiding these gap losses, e.g. Kammeyer (2011) or Gottschall et al. (2012), the results have not yet been transferred to small axial turbines using a VTG, marking the second major objective of this paper.

Requirements

The inital step in the process of designing and implementing the VTG is to identify the available installation space. Therefore, a model of the turbine from Sagan et al. (2022a) is shown in Figure 1. It can be seen that the oversized wastegate leaves insufficient space for the implementation of the VTG, despite the selection of the smallest commercially available wastegate. The authors are aware that this is a suboptimal solution and that the layout leaves considerable room for improvements. For example, the flow bypass could be implemented with a specially designed wastegate that directly connects the exhaust manifold of the engine to the turbine casing, thereby creating space for the control mechanism of the VTG in the axial direction (see shaded areas in Figure 1). This area is, therefore, regarded as the available installation space for the VTG, although the redesign of the layout is not within the scope of this paper. The small size of the stator is a direct consequence of the requirement to provide high compressor boost pressures at high exhaust gas densities during lean-burn operation. However, due to the small dimensions of the stator, the implementation of the VTG is quite challenging and requires a compact design. Simultaneously, the VTG is exposed to harsh operating conditions with gas temperatures of up to 970 °C in stoichiometric engine operation and must, therefore, be highly robust.

Concerning the required VTG pivot angle range, preliminary 1D engine simulations in combination with preliminary 3D CFD simulations of the initial turbine design without radial gaps resulted in a pivot angle range of

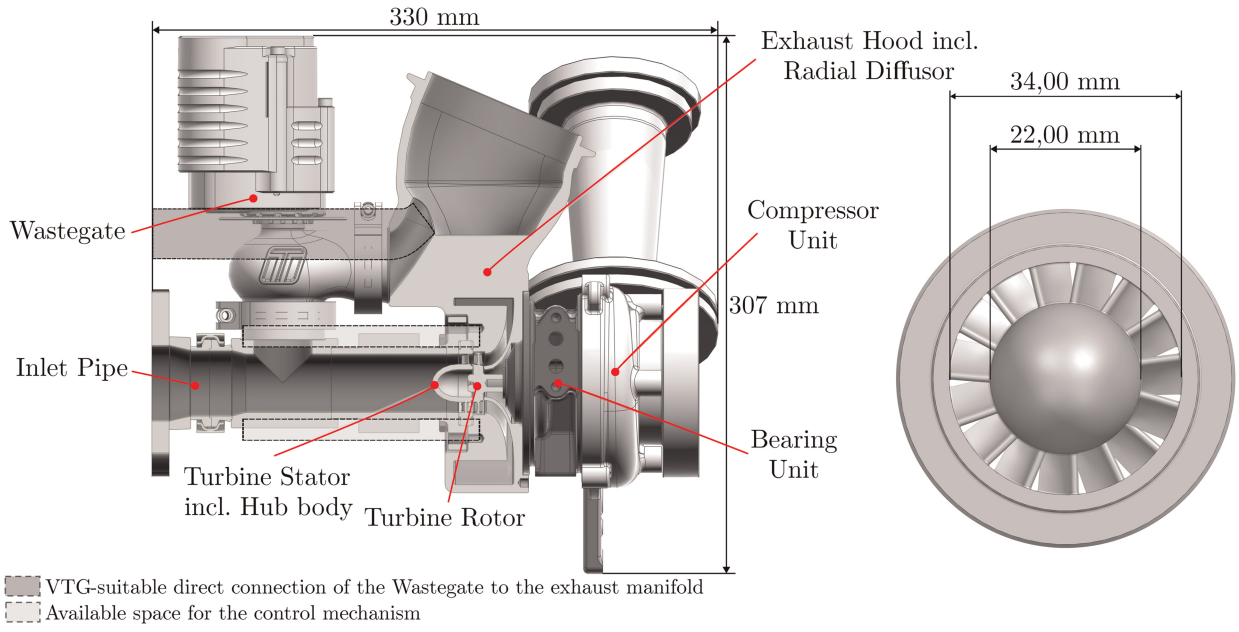

Figure 1. Cross-section of the turbine and stator from Sagan et al. (2022a).

−10° to 5° (Sagan et al., 2022b), whereby the negative sign indicates the closing and the positive sign the opening of the VTG (compare Figure 2b). Since the simulations are done without radial gaps, the secondary flow losses are underestimated, likely resulting in a higher actual required pivot angle range. Therefore, an estimated safety margin of 5° is added to the range determined above, resulting in a targeted pivot angle range of 20°.

VTG design

The subsequent objective in the VTG design is to find a suitable mechanism for adjusting the pivoting vanes. In this paper, a simple mechanism is selected with a linear actuator that rotates the vanes via levers. Although the control range is limited by the collision of adjacent levers, this concept can provide the targeted pivot angle range of 20°. Next, the vanes are rotatably mounted in the turbine inlet wall, which means that they can no longer be used to support the hub body. Struts are, therefore, installed in front of the stator. Since the hub body prohibits an installation from the inside of the inlet, the vanes must be installed from the outside. This requires a bore diameter of at least as large as the chord length of the vanes, which leads to further restrictions. To prevent the collision of the vanes in the inlet wall, a minimum circumferential distance between the holes must be maintained. However, this cannot be done with 15 vanes (see Figure 2a). Therefore, the number of vanes is reduced down to 13, accepting a possible reduction in the machine performance.

Due to the small vane heights of only 6 mm, even small radial gaps are expected to have a significant impact on the turbine's performance and choke characteristic. To minimize these losses, coin-shaped disks are added to seal the vane ends. While the disk can cover the entire vane on the shroud side, space limitations prevent the full sealing on the hub side for vane numbers >10 (see Figure 2b). However, preliminary studies with vane numbers of 10 or less showed a major impact on the turbine's choke characteristic and would entail extensive and undesirable changes to the vane design. At the same time, cascade test in the literature showed that stators with partly-sealed gaps can achieve the same efficiencies as fully sealed gaps (Gottschall et al., 2012). Based on these results, it is decided to keep the 13 vane (13V) design and only partially seal the hub-sided gap. A vane with the disks attached is shown in Figure 3a. However, the reduction in the number of vanes clearly requires an aerodynamic adjustment of the vanes in order to achieve the choke characteristics of the original turbine design.

With the number of vanes set, the vanes can be inserted from the outside of the inlet and secured radially with retaining rings. By attaching the levers to the vanes, an interface is created for the connection to the control mechanism. Figure 3b shows a possible solution following the approach of using levers with a guide groove. In this configuration, the actuator-induced linear movement of the ring is converted into a rotation of the vane. However, it should be noted that this is only a preliminary design, and the mechanism could be further optimized, particularly with regard to the comparatively large axial installation space required. Also, potential leakage flow has not yet been taken into account in this design.

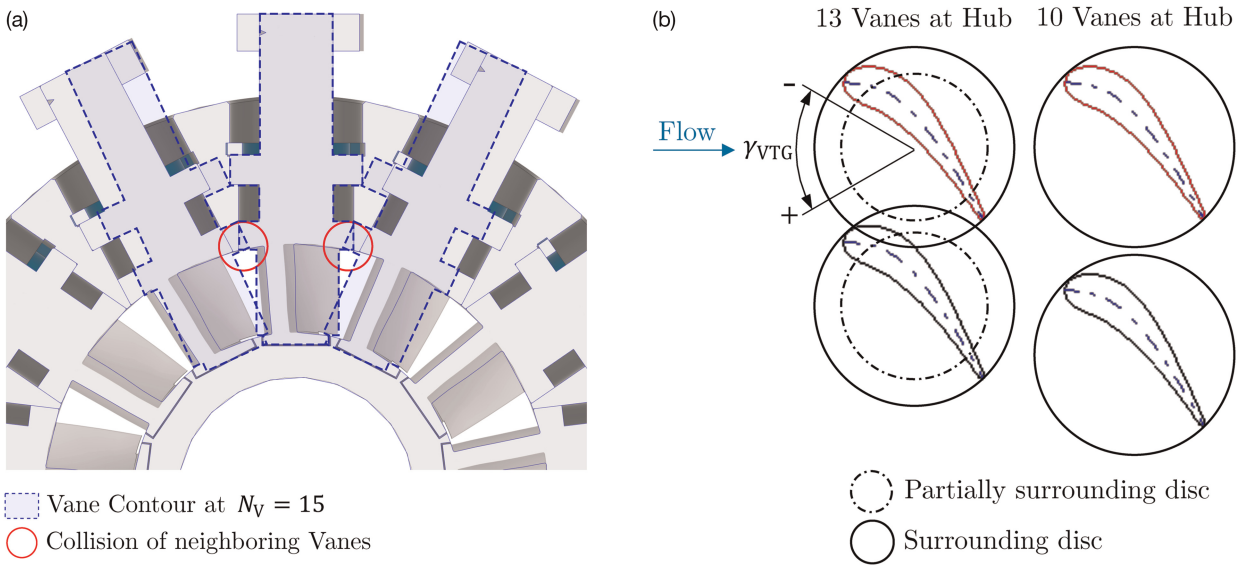

Figure 2. Space limitations for the VTG design. (a) Limitations due to the mounting in the inlet and (b) Limitations due to coin-like seals at the hub.

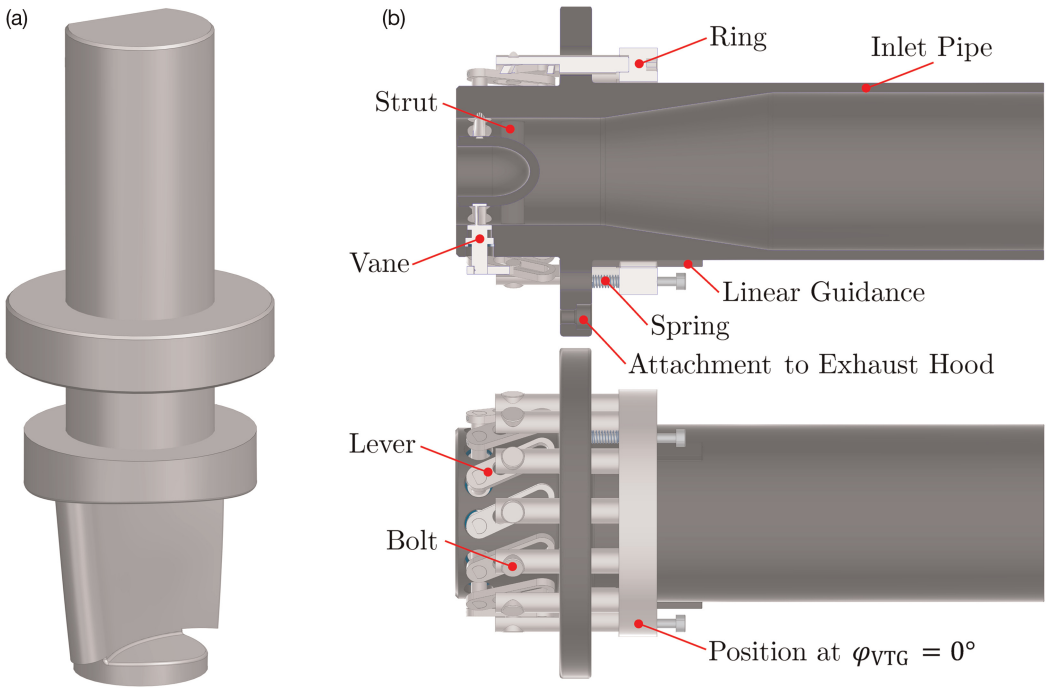

Figure 3. Draft of the VTG design. (a) Vane with applicated disks and (b) Control mechanism.

Vane redesign

In order to meet the characteristics of the initial turbine without a gap, CFD simulations are performed in Ansys CFX based on the numerical setup from Sagan et al. (2022a). It consists of the turbine inlet, the stator, the rotor, and the turbine exhaust hood with its integrated diffuser unit. This setup is updated with the revised stator geometry and the reduced number of vanes, but without hub-gaps in order to save time with the meshing. The meshing of the stator is done using the ICEM CFD module of Ansys. In order to estimate the error of the new stator mesh due to the spatial discretization, a mesh sensitivity study is performed using two systematically refined stator meshs with a refinement rate of $r = 1.8$. Next, the grid convergence index (GCI, Roache, 1998) is evaluated for the total pressure loss coefficient ζ as a metric for assessing the losses occurring in the stator.

$$\zeta = \frac{p_{t,in} - p_{t,out}}{p_{t,in} - p_{s,out}} \tag{2}$$

The calculations converged to an order of 2.65 and indicated a GCI value of 1.7% for the medium mesh, leading to a 95%-confidence interval of $\zeta = 0.939 \pm 0.016$. Given the computational effort and the achieved accuracy for the upcoming CFD simulations, this is deemed to be appropriate. Further results of the grid convergence study and a picture of the new stator mesh are provided in Table A1 and Figure A1 in the appendix.

With the updated model, the vane redesign is tackled to match the choke characteristic of the old and new stator design. As demonstrated by Sagan et al. (2022a), the critical operating range for the lean operation is within the lower engine speed range. Consequently, this was the basis for the selection of the aerodynamic design point (ADP, see Table 1). The ADP is, thus, utilized and investigated for the redesign of the stator with a VTG rack angle of $\gamma_{VTG} = 0°$. The results for the flow fields at the mid span of the stators are shown in Figure 4.

The direct comparison reveals a significant shift of the suction-sided flow separation for the 13V configuration in the area of the TE. As a result, larger wake areas can be observed. Moreover, the flow turning is reduced, thereby increasing the incidence at the rotor inlet. This can be seen by the rotor inlet flow angles $\beta_{rot,in}$ and the increased Zweifel coefficients in Table 2. The Zweifel coefficient can be understood as an indicator for the blade loading, whereby it relates the skin friction losses and the separation losses to the solidity of the stator. It is evaluated by

$$C_Z = 2 \cdot \frac{t}{l_{ax}} \sin \alpha_{out}{}^2 \cdot (\cot \alpha_{out} - \cot \alpha_{in}), \tag{3}$$

where t is the spacing between the vanes, l_{ax} is the axial chord length, and α is the flow angle (Zweifel, 1945). Since there is a minimum loss setting between the two loss mechanisms, wherein the Zweifel coefficient is

Table 1. Boundary conditions of the ADP.

Parameter	Value	Unit
Total inlet pressure $p_{t,in}$	1.7	bar
Total inlet temperature $T_{t,in}$	722	K
Rotational speed n	148,700	min^{-1}
Static outlet pressure $p_{s,out}$	1.1	bar

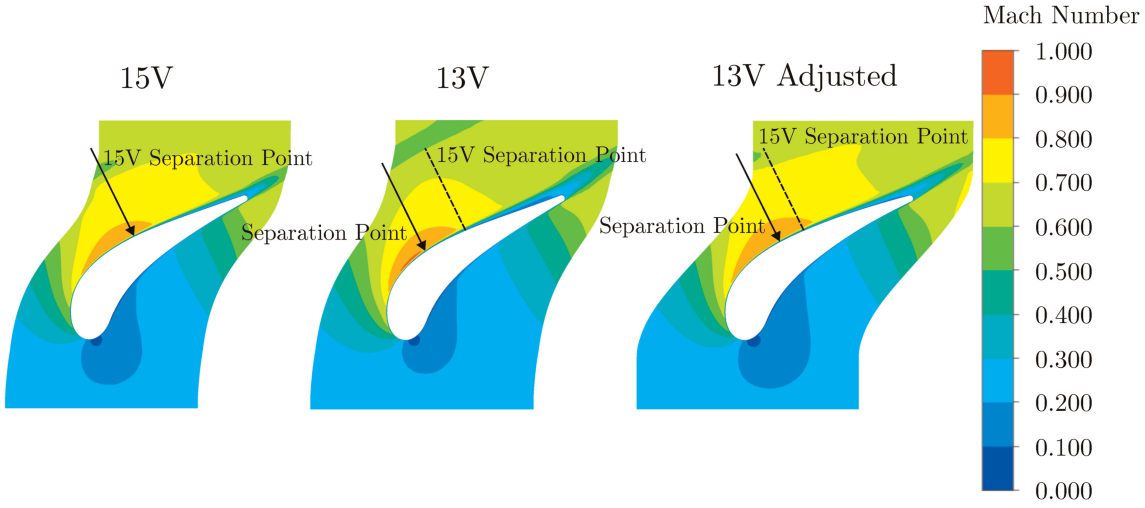

Figure 4. Flow field at the mid span of the initial 15V design from Sagan et al. (2022a), the unchanged 13V design, and the adjusted 13V design colored by the Mach Number.

Table 2. Rotor inlet flow angles $\beta_{rot,in}$ and Zweifel coefficients C_Z at the hub, mid, and tip span at γ_{VTG} 0=°.

Span	$N = 15$		$N = 13$		$N = 13$ (adj.)	
	$\beta_{rot,in}$	C_Z	$\beta_{rot,in}$	C_Z	$\beta_{rot,in}$	C_Z
Tip	75.3°	1.26	85.3°	1.61	77.9°	1.51
Mid	54.5°	0.99	63.7°	1.25	55.0°	1.15
Hub	44.1°	0.77	48.3°	0.92	43.4°	0.84

minimized, it can be used to determine the optimum solidity as a function of α_{in} and α_{out}. For current turbine designs, it is located between values of 0.9 and 1.2 according to Wilson and Korakianitis (2014). However, the combination of both the increased separation losses and the increased rotor incidence in the 13V design causes an efficiency loss of 1.2%-pts compared to the initial 15V design.

Concerning the mass flow rates, the increased cross-section of the 13V configuration yields a 7.2% higher mass flow rate of now 48.7 $g\,s^{-1}$ compared to the initial 45.2 $g\,s^{-1}$. To reduce this discrepancy, the trailing edge (TE) control points are gradually shifted in the circumferential direction until the mass flow rate of the initial design is achieved. This is regarded as a fairly simple but effective approach, since it changes the flow outlet

angle and also slightly increases the stator solidity. After a TE shift of 1.25°, the absolute deviation of the mass flow rate is already only 0.1 g s^{-1} (≈0.2). This is considered as sufficiently low to meet the engine's requirements. Furthermore, the rotor inlet flow angles are restored to a level approaching that of the initial design (compare Table 2) and the separation point on the suction side of the vane is shifted back towards the TE area, which reduces the wake areas. The aforementioned effects are illustrated for the mid span in Figure 4. As a consequence, the efficiency losses compared to the 15V configuration can be reduced down to 0.4%-pts. With regard to the losses, the next logical modifications would be to further adapt the vane chord length and the vane outlet angles $\alpha_{stat,out}$ to match C_Z and $\beta_{rot,in}$ with the initial design. However, the available circumferential space prevents longer chord lengths and since the rotor flow angles are already very similar to the initial design, the vanes are left without further modifications at this stage.

Given that the previous investigations are carried out without the radial gaps at the LE and TE in the hub area of the vane, it is imperative to examine the influence of these gaps on the choke characteristic to examine whether further adjustments to the blade design are necessary. The gap height is set to 0.175 mm as this is the gap required to allow the vanes to rotate. The evaluation shows that the gaps only lead to minor mass flow rate increases of 0.4 g s^{-1} and additional efficiency losses of 0.2%-pts. To counteract the mass flow rate deviation, the profile thickness is slightly enlarged by 0.1 mm at all vane spans, without changing the LE and TE thickness. As a result, the mass flow rates of the design without gaps are achieved. With regard to the efficiency, the thickness adjustments caused no further efficiency losses. Thus, the vane redesign is completed and the influence on the turbine performance map can be investigated. A visual comparison of the initial and the adjusted vane designs is provided in Figure 5.

Seal effects

This section addresses the evaluation of the turbine's performance in light of the implemented modifications and the effects of the seals. To distinguish the effects of the seals and the effects of the reduced number of vanes, in addition to the initial 15V design and the adjusted 13V design with partial gaps (13VPG), two further configurations are created based on the adjusted 13V design—one with a constant hub gap of 0.175 mm (13VCG) and one with no gap (13VNG). The three 13V configurations investigated are shown in Figure 6. The evaluation of the turbine performance is conducted on a single speed line at $n_{red} = 4{,}835$ min^{-1} K$^{-0.5}$ for the $\gamma_{VTG} = 0°$ VTG rack angle and all 13V configurations are compared to the initial 15V design. By plotting the corresponding mass flow rate deviations in percentage,

$$\Delta\dot{m}_{red,rel} = \frac{\dot{m}_{red,13V} - \dot{m}_{red,15V}}{\dot{m}_{red,15V}}, \tag{4}$$

it can be seen that the 13VNG design nearly matches the mass flow rates of the 15V design. This is also the case for the 13VPG design - even though its mass flow rates are up to 0.5% higher than those of the no-gap design. In contrast the 13VCG design exhibits significant deviations of more than 2.5%.

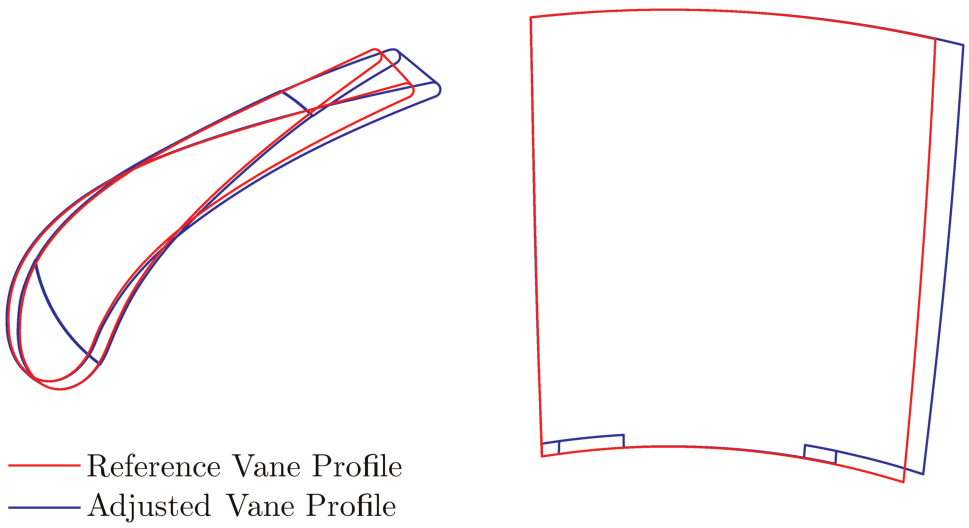

Figure 5. Visualization of the vane changes to match the choke characteristic.

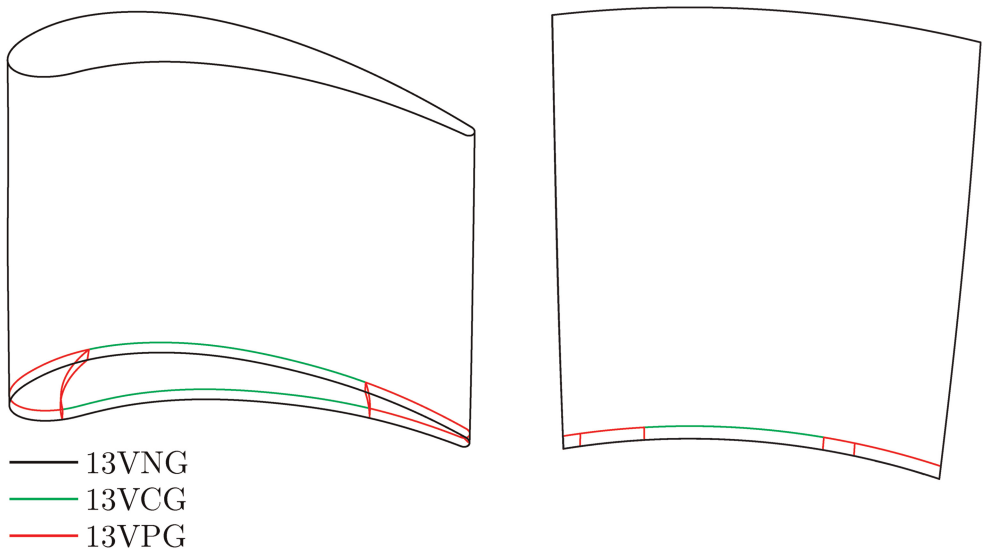

Figure 6. Visualization of the 13VPG, 13VNG and the 13VCG design.

While the differences are relatively small for low expansion ratios, they increase with an elevated expansion ratio. The reason for that are the larger passage throat areas A_{Throat} of the 13V designs, which are attributed to setting the mass flow rate instead of A_{Throat} as the reference parameter for the vane adjustments. At first glance, unequal throat areas may appear counterintuitive to achieve identical mass flow rates of the two designs. This would, of course, be the case in perfectly frictionless flow. However, in practice, losses must be taken into account, which affect the remaining terms in the continuity equation - namely, density and flow velocity. Since the product of both is a function of the total pressure p_{t} and the static pressure p_{s}, the mass flow rate depends also on the total pressure losses caused by the stator. This can be observed by the deviations of the 13VNG design at small expansion ratios in Figure 7a. Even though the design has a larger throat area than the initial 15V design, the mass flow rates are slightly lower for expansion ratios $\pi_{\mathrm{T,ts}} < 1.8$. By plotting the differences in p_{t} and p_{s} at the stator outlet in Figure 8b, it can be seen that this is attributed to the increased total pressure losses of the 13VNG design, thus, decreasing the $\rho \cdot c$ term in the continuity equation. Additionally, a strong correlation is evident between the mass flow rate deviations and the projected gap area A_{PGA} (compare Figures 7a and 8a). While the 13VPG design shows an almost constant offset, the deviations for the 13VCG design increase significantly with increasing expansion ratios. This phenomenon can be explained by the bypassing of the flow cascade by unturned tip leakage flow (Figure 9), which is described in Kammeyer et al. (2010a) as axial blow-by effect. As a result of the seal in the area of the strongest vane curvature, this effect can be significantly reduced. It can, therefore, be stated that partial seals in VTGs represent an effective way to increase the range of coverable mass flow rates.

Also in the context of the efficiencies, the ability of the partial seals to maintain the turning of the flow and, thus, to maintain the blade loading in the hub region proves to be a very effective way to reduce losses. As the

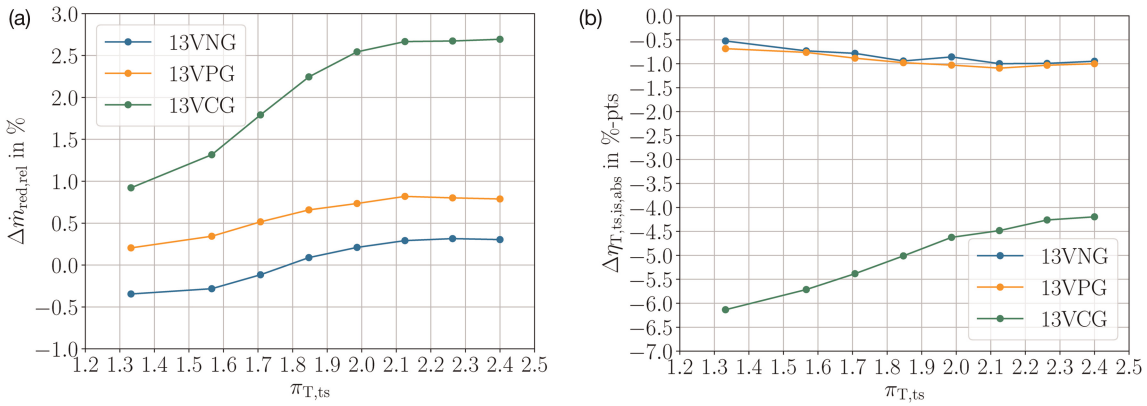

Figure 7. Deviations from the 13VPG, the 13VNG, and the 13VCG to the 15V design. (a) Relative mass flow rate and (b) Efficiency.

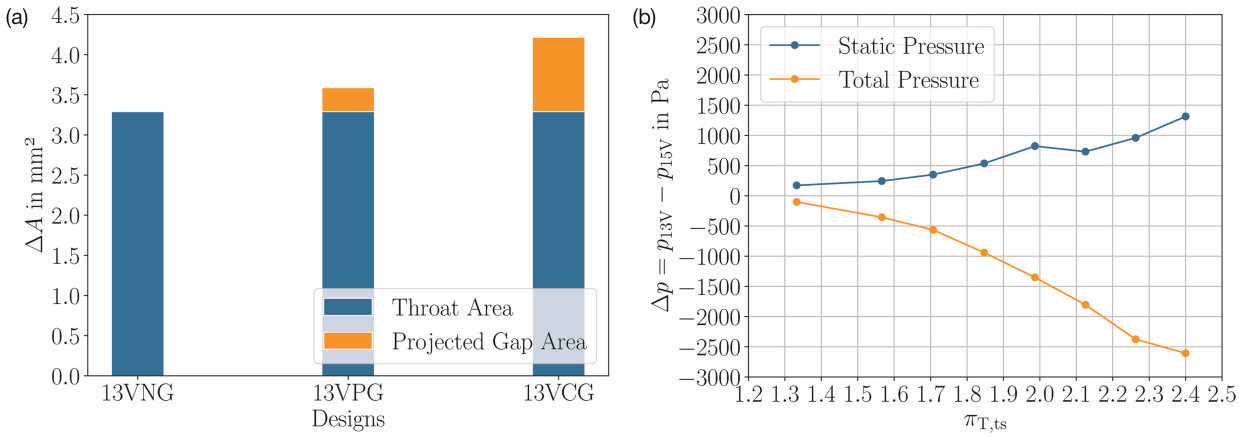

Figure 8. Factors influencing the reduced mass flow rate of the vane designs. (a) Comparison of the throat area and the projected tip gap area and (b) Absolute stator outlet pressure differences from the 13VNG to the 15V design.

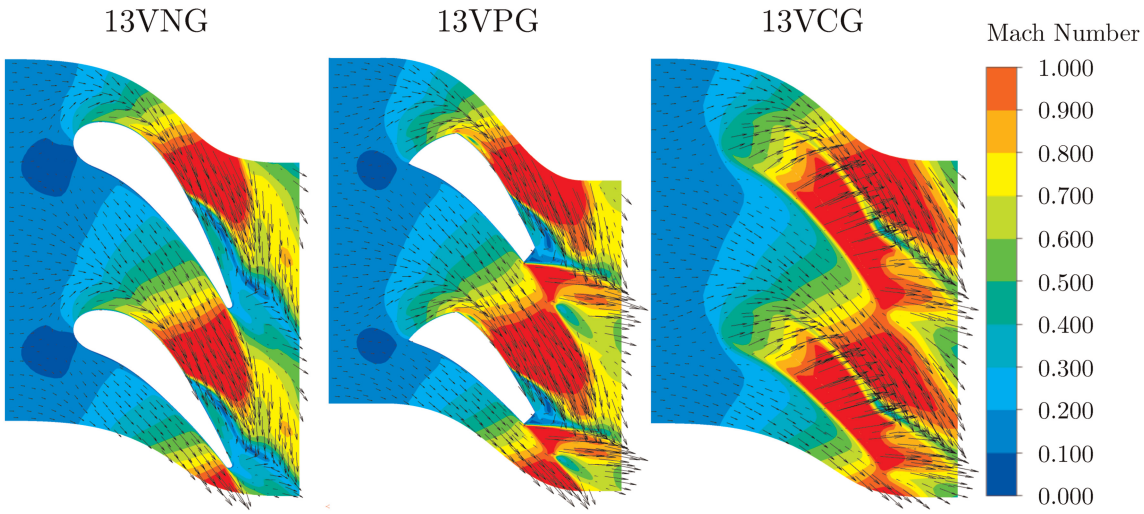

Figure 9. Flow field within the hub-gap contoured by the Mach number distribution at $\pi_{T,ts} = 2.4$.

efficiency levels and their deviations to the 15V design,

$$\Delta\eta_{is,abs} = \eta_{is,13V} - \eta_{is,15V}, \tag{5}$$

in Figure 7b illustrate, the 13VPG design is able to achieve deviations lower than 1.0%-pts. Compared to the efficiency losses of up to 6%-pts with the 13VCG design, this represents a notable improvement. Similar to previous publications in the context of larger cascade profiles (Gottschall et al., 2012), it can, thus, be demonstrated that the partial sealing of the gap in small turbomachines is sufficient to avoid the corresponding negative effects of the tip gaps on the efficiency. The remaining efficiency disadvantages observed in Figure 7b are, therefore, attributed to the larger profile losses of the adjusted stator.

Performance maps

In order to compare the performance maps of the 13VPG design with those of the initial 15V design, CFD simulations are performed for the four initially selected rack angles of $\gamma_{VTG} = 5°$, $0°$, $-5°$ and $-10°$. The results for the mass flow rate and the relative mass flow rate deviations to the 15V design are presented in Figure 10a. It can be seen that the relative mass flow deviations for the $\gamma_{VTG} = 0°$-position are low throughout the entire operating range. Depending on the expansion ratio, it ranges from +0.1% to +0.8% and averages at approximately +0.5%, confirming the vane redesign. The low deviations can also be maintained for the $\gamma_{VTG} = 5°$-position. Here, the values vary in the range from 0% to −0.5%. However, notable changes in the choke characteristic

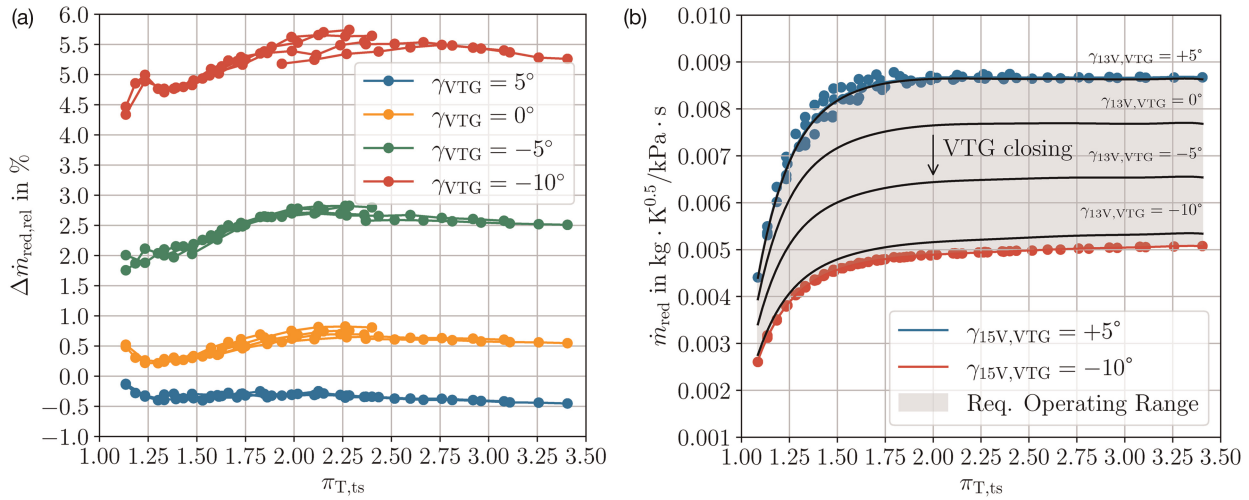

Figure 10. Investigation of the mass flow rates of the 13VPG and the 15V design. (a) Relative mass flow rate deviations of the 13VPG design to the 15V design and (b) Overview of the achievable operating range with 13VPG design.

can be observed at the positions $\gamma_{\mathrm{VTG}} = -5°$ and, in particular, $\gamma_{\mathrm{VTG}} = -10°$. While the deviation for the $\gamma_{\mathrm{VTG}} = -5°$-position is in the range of +3.0%, the values increase for $\gamma_{\mathrm{VTG}} = -10°$ up to +5.8% respectively.

These results can be explained by two causes. Firstly, the differences in the throat area between the 13VPG and 15V design increase when the vanes are pivoted, due to the reduction in the number of vanes. Secondly, the projected hub-gap area increases when the VTG is closed. Starting from the −5°-position, the difference in the throat area increases from initially +0.5% to +8.3% at the −10°-position. Concurrently, the projected hub-gap area increases by ≈35. That way, the 13VPG design is slightly limited in its operating range compared to the 15V design. This is illustrated by the offset of both $\gamma_{\mathrm{VTG}} = -10°$-lines in Figure 10b. However, given the distances between the VTG lines, the full engine operating range can be covered by using the entire pivoting range of $\Delta\gamma_{\mathrm{VTG}} = 20°$ to further close the VTG.

In addition to the choke characteristic, the turbine efficiencies and the associated deviations are shown in Figure 11. As with the choke characteristic, the results demonstrate a similar picture. The lowest losses are obtained for the $\gamma_{\mathrm{VTG}} = 5°$-position with values of −0.6%-pts at low expansion ratios and up to marginal efficiency advantages of 0.1%-pts at the highest expansion ratios. The latter could be due to the lower profile losses as a result of the reduced number of vanes, but given the differences in the values and the accuracy of the numerical model, it could also simply be due to numerical errors. However, when closing the VTG, the efficiency losses increase. The maximum losses are obtained at expansion ratios $\pi_{\mathrm{T,ts}} > 2.2$ with values of 1.2%-pts, 2.0%-pts, and 3.5%-pts for the $\gamma_{\mathrm{VTG}} = 0°$, −5°, and −10° positions, respectively.

Summarized, inefficiencies are apparent throughout the majority of the operating range, of which the losses at the $\gamma_{\mathrm{VTG}} = -5°$ and the $\gamma_{\mathrm{VTG}} = -10°$ positions in particular impair the transient operation. To reduce these

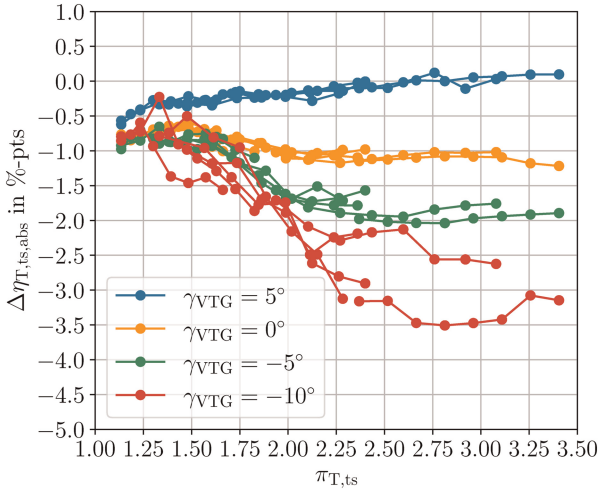

Figure 11. Absolute efficiency deviations of the 13VPG design to the 15V design.

losses, longer vanes would be required to reduce the Zweifel coefficients, which is prevented by the given geometric boundaries. Nevertheless, comparing the efficiency losses with those of the constant gap configuration, the results show that a reasonable design is found with the described method.

Conclusion

The present paper introduced a methodology for the subsequent implementation of a variable turbine geometry in an automotive T/C using a small axial turbine. The conceived control mechanism allowed the vanes to turn in a range of 20°. This required a reduction in the number of vanes from 15 to 13 due to the available circumferential space. To match the choke characteristic of the two designs, the TE was gradually shifted in circumferential direction and the vane thickness was increased. Both methods were found to be straightforward and effective for adjusting the mass flow rates. Another desirable adjustment would have been to increase the chord length to equalize the Zweifel coefficients; however, this was not feasible due to the limitations of the available installation space. Consequently, the 13V design showed a higher blade loading.

Subsequently, the effects of the radial gaps were investigated. Due to the small vane height, it was assumed that the gaps would have a significant impact on the turbine's performance. This assumption was confirmed by comparing distinct hub-gap designs along a specific speed line. It was found that constant relative hub-gaps of 3% lead to undesirable changes in both the mass flow rates (up to +2.8%) and the turbine efficiencies (up to −6%). However, by partially sealing the gap with a small disk at the vane's hub and by fully sealing it at the shroud, the mass flow rate deviations were significantly reduced down to +0.8%, while the efficiency disadvantages were almost entirely eliminated. This confirmed the findings from studies on large partially sealed cascades for small turbine stators and demonstrated that partial seals are able to extend the operating range of a VTG.

Finally, the VTG performance maps of the 13VPG and the 15V design were compared in terms of the coverable mass flow range and the turbine efficiencies. Thanks to the fully sealed tip-gap and the partially sealed hub-gap, the coverable mass flow ranges of both designs proved to be very similar. The 13VPG design requires only for the lower limit of the operating range a slightly larger pivoting angle range. With regard to the efficiency levels, the new 13VPG design showed a maximum disadvantage of only 1.2%-pts. for the most frequently used pivot angles of 5° and 0° and up to 3.5%-pts for the −10° position.

The results of this paper showed that the conceptual and aerodynamic design of the implemented VTG was successful. However, further aspects need to be examined in the future. For example, the sealing to the environment and the influence of thermal expansion have been ignored so far. Also, the utilization of the installation space still shows potential for optimization. These issues will be addressed in a subsequent study.

Appendix

Table A1. Parameter of the grid independence study.

Parameter	Value
r_{32}	1,8
r_{21}	1,8
$\zeta_{c,1}$	0,92912
$\zeta_{c,2}$	0,93868
$\zeta_{c,3}$	0,98260
GCI_1 in %	0.4
GCI_2 in %	1.7
GCI_3 in %	7.5

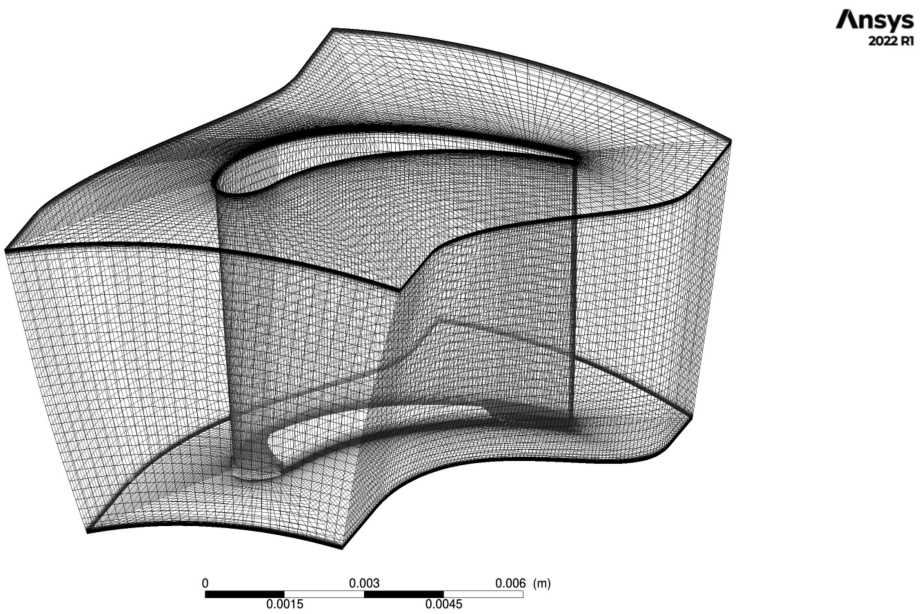

Figure A1. Medium mesh of the stator vane with partial gaps at the hub side.

Nomenclature

Greek Symbols

α	Absolute flow angle in °
β	Relative flow angle in °
η_{is}	Isentropic efficiency
γ_{VTG}	VTG rack angle in °
λ	Relative air-to-fuel ratio
π	Expansion ratio
ρ	Density in kg/m^3
ξ	Gap height
ζ	Total pressure loss coefficient

Other Variables

$\dot{m}$	Mass flow rate in kgs^{-1}
A	Area in mm^2
c	Absolute flow velocity in ms^{-1}
CZ	Zweifel coefficient
d	Diameter in mm
GCI	Grid convergence index
h	Height in mm
l	Chord length in mm
n	Rotational speed in min^{-1}
N_V	Number of vanes
p	Pressure in bar
r	Refinement rate
s	Thickness in mm
T	Temperature in K
t	Spacing between vanes in mm

Indices

abs	Absolute
in	Inlet
out	Outlet
red	Reduced
rel	Relative
rot	Rotor
s	Static
stat	Stator
T	Turbine
t	Total
V	Vane

Funding sources

1) Funder name: AiF eV, grant number: 22087 N/2
2) Funder name: FVV eV, grant number: 6014742
3) Funder name: FVV eV, grant number: 6014745.

Conflict of interests

Christoph Kuestner declares that he has no conflict of interest. Eike Helmsen declares that he has no conflict of interest. Joerg R. Seume declares that he has no conflict of interest.

References

Benstein E. H. and Wood H. J. (1964). Applications and performance levels of radial inflow turbines, Technical report, SAE Technical Paper.

Berenyi S. and Raffa C. (1979). Variable area turbocharger for high output diesel engines. SAE Technical Paper 790064, 1979. https://doi.org/https://doi.org/10.4271/790064.

Clasen K., Koopmans L., and Dahl D. (2018). Homogeneous lean combustion in a 2lt gasoline direct injected engine with an enhanced turbo charging system, Technical report, SAE Technical Paper.

Gottschall M., Vogeler K., and Mailach R. (2012). The effect of two different Endwall-Penny concepts for variable stator vanes in a compressor cascade. In: *Proceedings of the ASME Turbo Expo 2012: Turbine Technical Conference and Exposition. Volume 8: Turbomachinery, Parts A, B, and C.* ASME: Copenhagen, Denmark, pp. 83–93.

Kammeyer J. (2011). *Abgasturbolader mit Deckband zur Verringerung der turbinenseitigen Spaltverluste*. Hannover: Verlag Dr. Hut.

Kammeyer J., Natkaniec C., and Seume J. (2010a). Influence of tip-gap losses on the stage efficiency of downsizing turbocharger turbines. In: 9th International Conference on Turbochargers and Turbocharging - Institution of Mechanical Engineers, Combustion Engines and Fuels Group. Vol. 10. London, pp. 293–306.

Kammeyer J., Natkaniec C., and Seume J. R. (2010b). Tip leakage in small radial turbines: optimum tip-gap and efficiency loss correlations. In: *Turbo expo: power for Land, Sea, and Air*. Vol. 44007. Glasgow, UK: ASME, pp. 391–401. https://doi.org/10.1115/GT2010-22680.

Lei X., Li R., Xi Z., and Yang C. (2022). Effect of nozzle vane and rotor clearance on performance of variable nozzle turbine. *Journal of Thermal Science*. 31 (5): 1745–1758. https://doi.org/10.1007/s11630-022-1627-4.

Luszcz P., Takeuchi K., Pfeilmaier P., Gerhardt M., Adomeit P., et al. (2018). Homogeneous lean burn engine combustion system development–concept study. In: *18 Internationales Stuttgarter Symposium: Automobil-und Motorentechnik*. Wiesbaden: Springer Fachmedien Wiesbaden, pp. 205–223.

Natkaniec C. K., Kammeyer J., and Seume J. R. (2011). Secondary flow structures and losses in a radial turbine nozzle. In: *Turbo expo: power for Land, Sea, and Air*. Vol. 54631. Vancouver, British Columbia, Canada: ASME, pp. 977–987. https://doi.org/https://doi.org/10.1115/GT2011-46753.

Penny N. (1964). *Rover case history of small gas turbines*. SAE Transactions. 131–189. https://doi.org/10.4271/640012.

Roache P. J. (1998). *Verification and validation in computational science and engineering*. Vol. 895. Albuquerque, NM: Hermosa.

Sagan L., Küstner C., Eilts P., and Seume J. (2022a). Axial turbine turbocharger for charging a lean-burn gasoline engine. *SAE International Journal of Advances and Current Practices in Mobility*. 4 (2022-01-0377): 2342–2361. https://doi.org/10.4271/V131-99EJ-06.

Sagan L., Küstner C., Eilts P., and Seume J. (2022b). Single stage charging system for SI-engines operated with $\lambda = 2$ in the range of the WLTC. FVV Final Report H. 1298.

Sens M., Binder E., Benz A., Kramer L., Schultalbers M., et al. (2018). Pre-chamber ignition as a key technology for highly efficient SI engines-new approaches and operating strategies. In: *Proceedings of the 39th International Vienna Motor Symposium*, Vienna, Germany: Internationales Wiener Motorensymposium, pp. 26–27.

Storer J. and Cumpsty N. (1991). Tip leakage flow in axial compressors.

Wenz E., Pauls A., Thielen M., Todt A., and Eilts P. (2021). Exploiting SI engine efficiency through lean burn operation in combination with stroke extension, Miller timings and high compression ratios, Technical report, SAE Technical Paper.

Wilson D. G. and Korakianitis T. (2014). *The design of high-efficiency turbomachinery and gas turbines*. Cambridge, Massachusetts: The MIT Press.

Zaccardi J.-M. and Pilla G. (2019). Hydrogen as a combustion enhancer for highly efficient ultra-lean Spark-Ignition engines. *SAE International Journal of Advances and Current Practices in Mobility*. 2 (2019-01-2258): 401–414. https://doi.org/10.4271/V129-99EJ-01.

Zweifel O. (1945). The spacing of turbo-machine blading, especially with large angular deflection. *Brown Boveri Review*. 32 (12): 436–444.